Molecular Biology of the Cell
Vol. 19, 30–40, January 2008

LARG and mDia1 Link $G\alpha_{12/13}$ to Cell Polarity and Microtubule Dynamics

Polyxeni Goulimari,* Helga Knieling,* Ulrike Engel,† and Robert Grosse*

*Institute of Pharmacology, University of Heidelberg, 69120 Heidelberg, Germany; and †Nikon Imaging Center at the University of Heidelberg, Bioquant, 69120 Heidelberg, Germany

Submitted November 27, 2006; Revised October 5, 2007; Accepted October 10, 2007
Monitoring Editor: Martin A. Schwartz

Regulation of cell polarity is a process observed in all cells. During directed migration, cells orientate their microtubule cytoskeleton and the microtubule-organizing-center (MTOC), which involves integrins and downstream Cdc42 and glycogen synthase kinase-3β activity. However, the contribution of G protein-coupled receptor signal transduction for MTOC polarity is less well understood. Here, we report that the heterotrimeric $G\alpha_{12}$ and $G\alpha_{13}$ proteins are necessary for MTOC polarity and microtubule dynamics based on studies using $G\alpha_{12/13}$-deficient mouse embryonic fibroblasts. Cell polarization involves the $G\alpha_{12/13}$-interacting leukemia-associated RhoGEF (LARG) and the actin-nucleating diaphanous formin mDia1. Interestingly, LARG associates with pericentrin and localizes to the MTOC and along microtubule tracks. We propose that $G\alpha_{12/13}$ proteins exert essential functions linking extracellular signals to microtubule dynamics and cell polarity via RhoGEF and formin activity.

INTRODUCTION

Polarity is a multifaceted and necessary aspect of cellular function. Directed cell migration during development and differentiation, apicobasolateral polarity in epithelial cells, and axon specification in neuronal cells are only a few examples of the far-reaching impact of cell polarity. These processes require tightly regulated asymmetric signaling of membrane trafficking, cell adhesion, and cytoskeleton dynamics (Fukata *et al*., 2003). Polarization of the microtubule-organizing-center (MTOC) and microtubule reorganization represent hallmarks of the polarized phenotype of a directionally migrating cell centrally involving the monomeric GTPase Cdc42 (Kiosses *et al*., 1997; Etienne-Manneville and Hall, 2003).

MTOCs such as the centrosome are potent microtubule nucleators, and they have the ability to organize and polarize microtubules in arrays (Zimmerman *et al*., 1999). It is suggested that different proteins are involved in organizing and nucleating microtubules at the centrosomes. Pericentrin, one of the first characterized proteins found at the pericentriolar material (Doxsey *et al*., 1994), forms a complex with γ-tubulin at the centrosome. In this complex, pericentrin is bound to the centrosome lattice and to γ-tubulin complexes, which directly nucleate microtubules (Dictenberg *et al*., 1998; Luders and Stearns, 2007).

In migrating cells, microtubule dynamics are controlled in a spatiotemporal manner (Akhmanova and Hoogenraad, 2005). In turn, other regulatory components are dependent on microtubule dynamics, such as local activation of RhoA, successful transport of membrane vesicles and focal adhesion turnover (Wittmann and Waterman-Storer, 2001; Moissoglu and Schwartz, 2006; Birkenfeld *et al*., 2007). These events are likely regulated by proteins on microtubule plus-ends (Galjart and Perez, 2003). A number of microtubule plus-end–binding proteins have been described, such as adenomatosis polyposis coli (APC), cytoplasmatic linker proteins, cytoplasmatic linker protein-associating proteins, dynein/dynactin complex, and EB1 (Galjart and Perez, 2003; Mimori-Kiyosue and Tsukita, 2003). A conserved function of EB1 is to elongate microtubules (Ligon *et al*., 2003). EB1 can associate with APC (Su *et al*., 1995) and stabilizes the microtubule lattice seam (Sandblad *et al*., 2006).

In *Drosophila melanogaster* Schneider cells, DRhoGEF2 is involved in apical-basal cell polarity; DRhoGEF2 contains a regulator of G protein signaling (RGS) domain that is known to bind activated α subunits of heterotrimeric G proteins. DRhoGEF2 colocalizes with γ-tubulin at the centrosome, and it is transported to the cell cortex along microtubules tips, in an EB1-dependent manner (Rogers *et al*., 2004).

RhoA has been implicated in cell polarity; genetic studies in *D. melanogaster* demonstrate that the *Drosophila* RhoA homologue is required for tissue polarity (Strutt *et al*., 1997). In *Xenopus laevis*, activation of RhoA and the formin Daam1 is involved in planar cell polarity during gastrulation (Habas *et al*., 2001). Furthermore, the RhoA-effector and potent actin nucleator mDia1 has been shown to play essential roles in directional migration of mammalian cells (Faix and Grosse, 2006). Mammalian Dia1 localizes to membrane ruffles (Watanabe *et al*., 1997) and to the front of migrating fibroblasts in a $G\alpha_{12/13}$ protein-dependent manner (Goulimari *et al*., 2005). In addition, the cytoskeletal scaffold and cell polarity protein IQGAP1 was recently demonstrated to recruit mDia1 to the leading front of migrating cells (Brandt *et al*., 2007).

This article was published online ahead of print in *MBC in Press* (http://www.molbiolcell.org/cgi/doi/10.1091/mbc.E06–11–1045) on October 24, 2007.

Address correspondence to: Robert Grosse (robert.grosse@pharma.uni-heidelberg.de).

Abbreviations used: EB1, end binding protein 1; FH2, formin homology 2 domain; LARG, leukemia associated RhoGEF; MEF, mouse embryonic fibroblast; MTOC, microtubule-organizing center; TIRF, total internal reflection fluorescence.

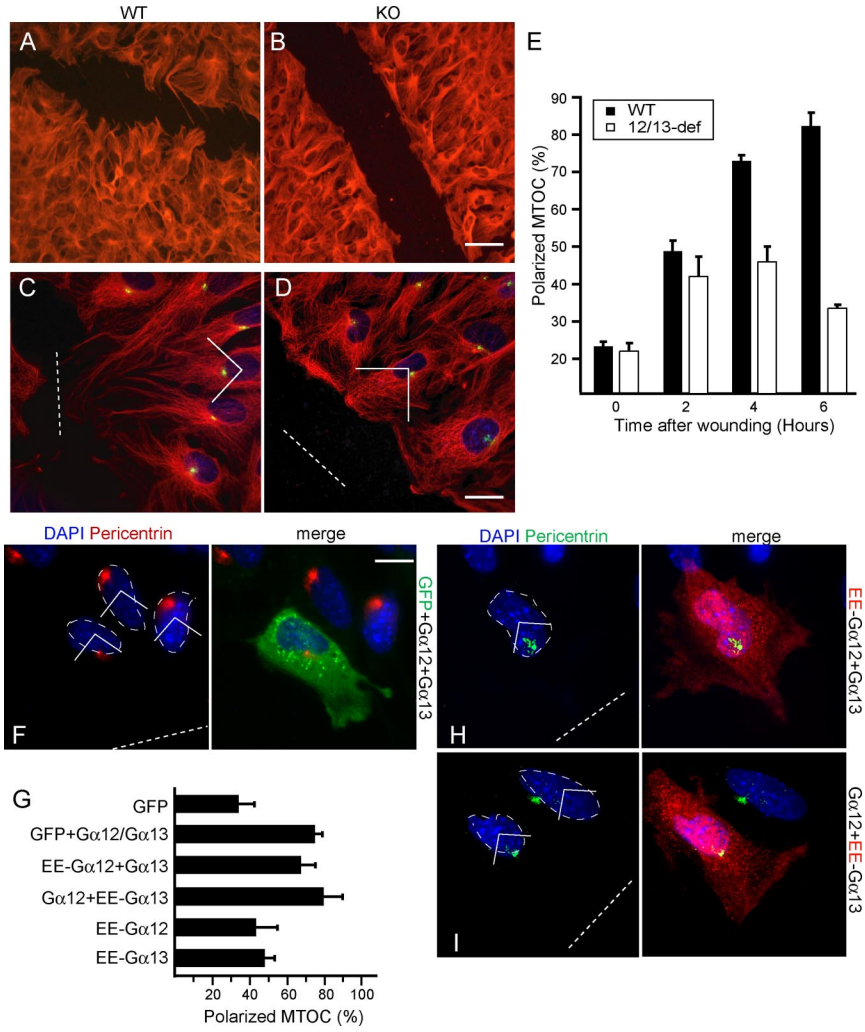

Figure 1. $G\alpha_{12/13}$ is required for MTOC polarization. (A) WT and (B) KO MEFs were stained with α-tubulin (red) antibody to visualize the microtubule cytoskeleton 6 h after wounding. Bar, 30 μm. (C) WT and (D) KO cells were stained with anti-α-tubulin (red), anti-pericentrin to visualize the MTOC (green), and 4,6-diamidino-2-phenylindole (DAPI) to visualize the nucleus (blue). Bar, 20 μm. (E) The percentage of WT (■) and KO MEFs (□) in the front row having their MTOC in the forward-facing quadrant (shown) was assessed at the indicated time after wounding. We scored 200 cells per time point. Data represents means ± SEM of five independent experiments. (F) Representative image of a KO cell microinjected with GFP, WT $G\alpha_{12}$, and WT $G\alpha_{13}$ and stained for MTOC (green) and DAPI (blue). Bar, 10 μm. (G) Quantification of positive MTOCs in cells expressing the indicated constructs. (H) Representative image of a KO cell expressing EE-$G\alpha_{12}$(red) and $G\alpha_{13}$ after comicroinjection and stained for DAPI (blue) and pericentrin (green) (I) Representative image of a KO cell expressing EE-$G\alpha_{13}$ (red) and $G\alpha_{12}$ after comicroinjection and stained for DAPI (blue) and pericentrin (green). Results represent the means ± SEM of three independent experiments (70 cells total). Wound gaps are indicated by dotted lines.

The importance of heterotrimeric $G\alpha_{12/13}$ proteins for RhoA-mediated actin dynamics, oncogenic transformation, or cancer cell invasion is well established (Gudermann *et al.*, 2000; Kelly *et al.*, 2006a,b); however, their roles in microtubule dynamics and the regulation of the microtubule cytoskeleton have not been investigated. $G\alpha_{12/13}$ proteins are essential for development because double-deficient mice die at embryonic day 8.5 (Offermanns, 2003), and suppression of $G\alpha_{12/13}$ function disrupts convergence and extension during zebrafish gastrulation (Lin *et al.*, 2005). We previously demonstrated that $G\alpha_{12/13}$ proteins are necessary for wound-induced cell migration through localized Rho-mDia1 function (Goulimari *et al.*, 2005). Here, we analyze the role of $G\alpha_{12/13}$ in cell polarity by assessing MTOC reorientation and microtubule dynamics in mouse embryonic fibroblasts (MEFs) lacking these G proteins. Our findings demonstrate that $G\alpha_{12/13}$ critically regulate microtubule dynamics and MTOC polarization through LARG, which belongs to the family of RhoGEFs containing an RGS domain that directly binds to $G\alpha_{12/13}$ proteins (Fukuhara *et al.*, 2000; Tanabe *et al.*, 2004; Kreutz *et al.*, 2007). We find that LARG associates with pericentrin and localizes to the MTOC and along microtubule tracks. These data suggest an important biological role for LARG in the control of cell polarity downstream of $G\alpha_{12/13}$.

MATERIALS AND METHODS

Materials

Antibodies used were as follows: α-RhoA (26C4) and α-LARG (N-14) were from Santa Cruz Biotechnology (Santa Cruz, CA); α-EB1, α-Rac, α-Cdc42, α-p140Dia1, and α-glycogen synthase kinase (GSK)-3β were from BD Transduction Laboratories (Lexington, KY); α-pericentrin (MTOC) was from Eurogentec (Seraing, Belgium); α-α tubulin, nocodazole, and anti-c-myc-agarose were from Sigma-Aldrich (St. Louis, MO); and α-GSK-3β (serine 9) and α-β catenin were from BioSource International (Camarillo, CA). The Alexa 350-phalloidin and anti-mouse Alexa 568 were from Invitrogen (Carlsbad, CA). Y27632 compound was from Calbiochem (San Diego, CA), and lysophosphatidic acid (LPA) was from BIOMOL Research Laboratories (Plymouth Meeting, PA). Anti-EE was from Covance (Hiss Diagnostics, Freiburg, Germany). The green fluorescent protein (GFP)-EB1 was a gift from Dr. J. Wehland (Helmholtz Centre of Infection Research, Braunschweig, Germany). All mDia1 and LARG constructs used in this study have been described previously (Goulimari *et al.*, 2005; Rosenfeldt *et al.*, 2006; Brandt *et al.*, 2007; Kitzing *et al.*, 2007). GFP-postsynaptic density 95/disc-large/zona occludens (PDZ)-RGS and GFP-RGS were generated by amplifying the cDNA from LARG encoding amino acids 72–556 and 348–556, respectively, by using the following primers: forward 5′-cgcgcgggatcctgcgtaatcatccagaaagat-3′ and reverse 5′-cgcgcggaattcttattttactcccaaatgcttcat-3′ for PDZ-RGS and forward 5′-cgccgcgg-gatccggacagtgcagctgtttcca-3′ for RGS. The polymerase chain reaction (PCR) products were ligated into an EFplink2-GFP vector.

Cell Culture and Wound Healing Assays

Cell culture procedure and wound-healing assays were described previously (Goulimari *et al.*, 2005). Briefly, confluent monolayers of starved cells were scratched once with a cut 10-μl tip. Cells were monitored using a CTR MIC microscope (Leica, Wetzlar, Germany). Pictures were acquired with a Leica

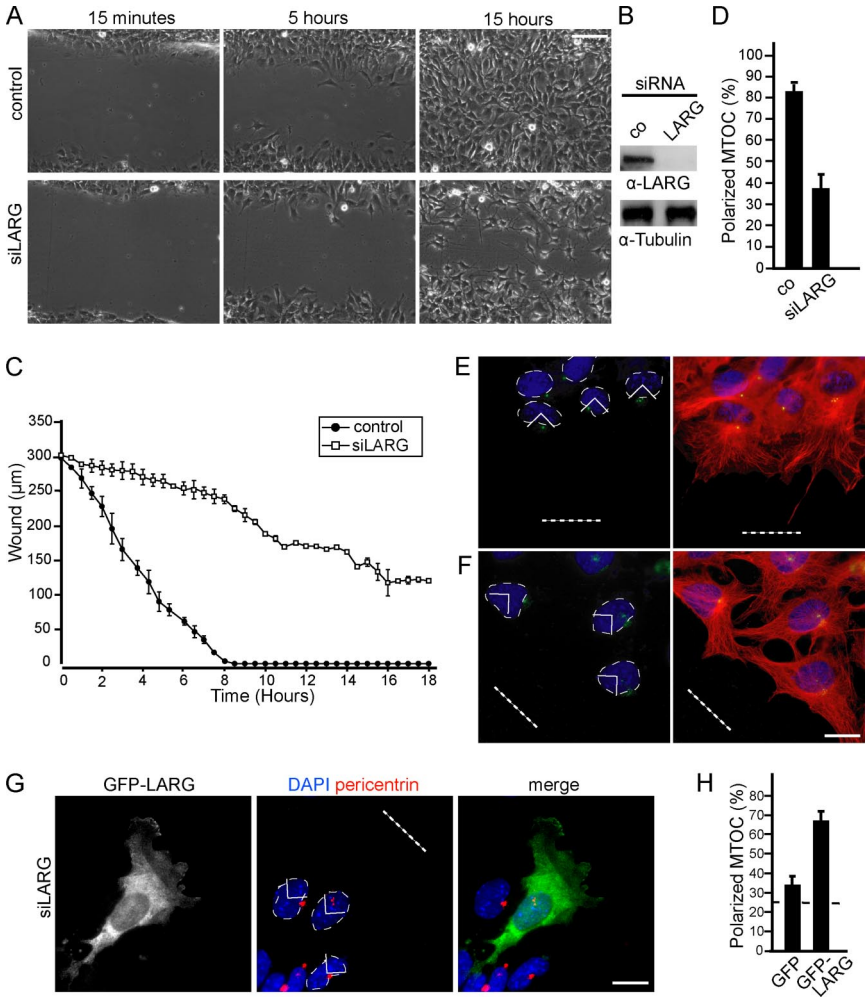

Figure 2. LARG is necessary for directed cell migration and MTOC polarization. (A) Representative phase contrast images from live-cell recordings (Supplemental Movies 1 and 2) of siRNA control transfected MEFs (top) or LARG siRNA transfected MEFs (bottom) at 15 min, 5 h, and 15 h after wounding. Bar, 50 μm. (B) Cell extracts were immunoblotted for LARG. (C) Statistical analysis of scratch-induced migration assays from 30-min interval live cell recordings; ●, control; □, siRNA against LARG. (D) Quantification of positive MTOCs in cells transfected with control siRNA or siRNA against LARG. Error bars in C and D represent SEM. Representative images of WT cells after control siRNA (E) or siRNA against LARG treatment (F) and stained for MTOC (green), DAPI (blue), and merged with α-tubulin (red). (G) Representative image of a cell microinjected with GFP-LARG (green; arrow) after the indicated treatment and stained for MTOC (red) and DAPI (blue). (H) Quantification of positive MTOCs in cells microinjected with GFP-LARG after treatment with siRNA against LARG. Data represent means ± SEM of three independent experiments (75 cells total). Bar, 10 μm. Wound gaps are indicated by dotted lines.

DC 350 FX camera using the Leica software FW4000. For statistical analysis, triplicates of wound distance were measured at three randomly defined wound gap locations in each frame. At least three independent experiments were used.

Knockdown of Mouse RhoA, mDia1, Cdc42, and LARG Induced by Small Interfering RNA (siRNA)

All siRNA sequences used are from IBA GmbH (Goettingen, Germany). The sequence for mDia1 siRNA has been published previously (Arakawa *et al.*, 2003; Goulimari *et al.*, 2005; Eng *et al.*, 2006; Yamana *et al.*, 2006). The siRNA sequence against RhoA was chosen according to Wang *et al.* (2003). siRNA corresponding to Cdc42 is as follows (5′-GCU GGU CAG AGC CAU GGA U UU-3′). The siRNA against LARG is the following (5′-AAA CCA AAU GUA UAG AGC U TT-3′), and it is located in the 3′ untranslated region (UTR). A control sequence (5′-CGC GUA GAA GAU GAA GUU GTT-3′) was purchased from IBA. Transfection of MEFs with siRNA duplexes (2 μg/μl) was performed using magnet-assisted transfection according to manufacturer's instructions (IBA) as described previously (Goulimari *et al.*, 2005). Cells were analyzed 48 h after siRNA transfection.

Immunofluorescence and Microscopy

Cells were stained as described previously (Grosse *et al.*, 2003), or they were fixed with ice-cold methanol for microtubule and MTOC staining. For calcium depletion, cells were grown in 10% fetal bovine serum (FBS) DMEM without calcium (Invitrogen) with the addition of 4 mM EGTA and 1 mM magnesium chloride, and then they were fixed and stained (Sahai and Marshall, 2002). Immunofluorescence micrographs were obtained with a Leica DC 350 F camera on a Leica DM IRE 2 microscope and Leica IM 50 software. For MTOC stainings, cells were fixed 6 h after wounding, and images were acquired on a Nikon Eclipse 90i upright automated microscope equipped with a Nikon DS-1QM cooled black-and-white charge-coupled device (CCD) camera and NIS Elements AR 3.20 software (Nikon, Tokyo, Japan). Positive MTOCs were scored using a 90° angle relative to the wound. Cells were analyzed 6 h after wounding, unless otherwise stated. Confocal images were acquired at a spinning disk confocal ERS-FRET (PerkinElmer Life and Analytical Sciences, Boston, MA) on a Nikon TE2000 inverted microscope (Nikon, Tokyo, Japan) equipped with a EM-CCD camera (Hamamatsu, Bridgewater, NJ) and UltraVIEW ERS software.

Microinjections

For rescue experiments, cells were scratched and after 4 h they were microinjected with the indicated proteins. Then, 1.5 h later, cells were fixed with 8% formaldehyde (FA) for 10 min at room temperature and stained for MTOC as described above. An Eppendorf Femtojet and Injectman micromanipulator attached to an Axiovert 135 microscope (Carl Zeiss, Jena, Germany) was used for microinjections. Concentration for all constructs was the following: GFP (0.05 μg/μl), wild-type (WT) Gα_{12} (0.05 μg/μl), WT Gα_{13} (0.05 μg/μl), GFP-LARG (0.2 μg/μl), Dia1-compl (0.05 μg/μl), ΔDAD (0.05 μg/μl), Δ750-770ΔDAD (0.05 μg/μl), flag-pcDNA3 (0.05 μg/μl), EE-Gα12 (0.2 μg/μl), EE-Gα13 (0.2 μg/μl), GFP-EB3 (0.05 μg/μl), GFP-PDZ-RGS (0.2 μg/μl), and GFP-RGS (0.2 μg/μl).

In Situ Rho Hybridization

For in situ Rho hybridization, cells were incubated with recombinantly purified GFP or GFP-rhotekin-Ras binding domain (RBD) (GFP-RBD). Generation of the probes and in situ Rho affinity assays have been described previously (Goulimari *et al.*, 2005). The following changes were made to the protocol. After fixation and permeabilization, cells were blocked in 5% FBS in phosphate-buffered saline (PBS) for 1 h. After blocking, the cells were preincubated with recombinantly purified monomeric red fluorescent protein (mRFP) (0.02 μg/μl) in 5% FBS/PBS for 1 h to block unspecific binding, followed by incubation with GFP-RBD (0.02 μg/μl). Software analysis (NISElements AR 2.30; Nikon) was used to subtract the mRFP background from the respective GFP-RBD image.

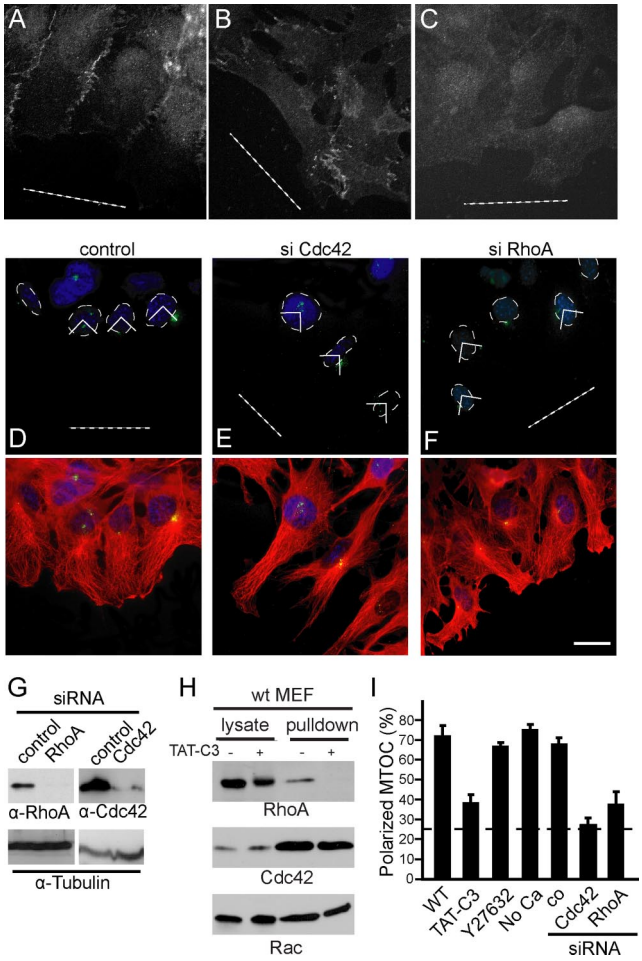

Figure 3. RhoA activity is required for MTOC polarization. WT MEFs (A and C) or $G\alpha_{12/13}$-deficient fibroblasts (C) were stained for cell junctions by using β-catenin antibody. (C) Cells were maintained in calcium-free medium before wounding to displace β-catenin from the cell-cell contacts (see *Materials and Methods*). (D–F) Representative images of cells stained for MTOC (green) and DAPI (blue) after transfection with siRNA against the indicated proteins. Merged images with α-tubulin (red) are shown. Dotted white line shows the wound. (G) Cell extracts were immunoblotted for the indicated proteins. (H) WT MEFs were maintained in 10% serum, and they were treated with TAT-C3. Cdc42 or Rac pull-down analysis was performed simultaneously with the Rho assay (as described in *Materials and Methods*). Western blot analyses of GST-RBD precipitates (pull-down) and of corresponding lysates are shown. (I) Quantification of positive MTOCs after the indicated treatment (see *Materials and Methods*). Data represent means ± SEM of three independently performed experiments (200 cells/treatment). Bar, 10 μm.

Total Internal Reflection Fluorescence Microscopy (TIRFM) and Analysis of Microtubule Dynamics

For TIRF microscopy, the cells were grown on glass-bottomed dishes (MatTek, Ashland, MA) until confluent. For immunocytochemistry, the cells were subsequently scratched and fixed with ice-cold methanol at the indicated times and stained for EB1 as described above, but they were maintained in a PBS solution, enabling internal reflection to take place. TIRF images were obtained on a Nikon TIRF setup with 488-nm and 561-laser excitation, a 60× PlanApo numerical aperture 1.45 objective on a TE-2000 equipped with an Orca-AG CCD camera (Hamamatsu) and NIS Elements AR 2.30 software (Nikon). For live-cell TIRFM, cells were scratched and 30 min later, leading edge cells were microinjected with GFP-EB1 (0.05 μg/μl) as described above. Time-lapse microscopy was performed 1 h later on the TIRF setup where cells were kept at 37°C with a Tokai Hit heating chamber. To monitor EB1 dynamics, time-lapse sequences were acquired at intervals of 3 s for a period of 5 or 10 min.

For quantification of microtubule advance rates, data were imported into ImageJ (http://rsb.info.nih.gov/ij/), and kymographs were created to visualize the displacement of the EB1 dashes. Kymograph analysis creates a time versus distance plot of intensity along the axis of a rectangular region of interest. A vertical trace indicates no displacement, and traces with shallow slopes indicate high velocity. Advance rates of microtubules were calculated by measuring angles of all distinguishable traces. Maximum projection images from time-lapse sequences were used to directly compare the EB1 tracks as well as manual tracking and velocity quantifications of EB1 and EB3 comets from epifluorescence movies were done with ImageJ.

For analysis of LARG localization with TIRFM, cells were grown on glass-bottomed dishes (MatTek) until confluent. Confluent cells were scratched, and 30 min later they were microinjected with GFP-LARG (0.2 μg/μl), fixed with 8% FA, and stained for α-tubulin.

Pull-Down Assays, Coimmunoprecipitions, and Western Blot Analysis

Lysates from wounded MEFs were subjected to RhoA pull-down assays by using agarose beads bound to glutathione transferase (GST)-rhotekin-RBD as described previously (Grosse *et al.*, 2000; Vogt *et al.*, 2003). Rac and Cdc42 activity assays were performed in parallel to RhoA pull-down by adding 1 μg/ml purified biotinylated Cdc42/Rac interactive binding peptide to the lysis reaction (Price *et al.*, 2003). Proteins were eluted with SDS-sample buffer and analyzed by SDS-polyacrylamide gel electrophoresis (PAGE). For Western blot detection of GSK-3β phosphorylation, the total lysates from GTPase activity assays were used in parallel. TAT-C3 treatment (0.2 μM) and treatment with Y27632 (10 μM) were performed for 18 h before cell wounding. Cell monolayers were lysed at the indicated times, and proteins were subjected to SDS-PAGE. Densitometric quantifications were analyzed in Adobe Photoshop CS2 (Adobe Systems, Mountain View, CA).

For interaction studies, human embryonic kidney (HEK) cells were transfected with 1 μg of myc-LARG for 48 h. Cell extracts were then subjected to immunoprecipitation and immunoblotting as described previously (Grosse *et al.*, 2003).

RESULTS

To analyze the microtubule cytoskeleton of $G\alpha_{12/13}$-deficient MEFs, we performed tubulin and MTOC stainings on scratch-wounded cell monolayers. Under 10% serum conditions, WT cells displayed polarized microtubules protruding toward the wound gap (Figure 1A) in contrast to $G\alpha_{12/13}$-deficient cells (KO) (Figure 1B). We then compared MTOC relocalization in scratched monolayers of WT or $G\alpha_{12/13}$-deficient MEFs (Figure 1, C and D). MTOC reorientation, although cell-type specific, typically occurs within 1–6 h (Fukata *et al.*, 2003). Within this time frame, most WT cells reorientated their MTOC in front of the nucleus toward the wound (Figure 1, C and E). However, the ability of the $G\alpha_{12/13}$-deficient cells to polarize the MTOC was strongly affected (Figure 1, D and E). This defect could be rescued after reintroduction of untagged or EE-tagged versions of $G\alpha_{12}$ and $G\alpha_{13}$ (Figure 1, F and G). $G\alpha_{12}$ or $G\alpha_{13}$ alone could not rescue MTOC reorientation in the KO cells (Figure 1G). EE-$G\alpha_{12}$ comicroinjected with $G\alpha_{13}$ and vice versa showed a dotty localization pattern (Figure 1, H and I) and efficiently rescued MTOC polarity (Figure 1G). Additional analysis revealed that the serum component LPA can alone promote polarized migration of fibroblasts as expected (Palazzo *et al.*, 2001), but not in cells lacking $G\alpha_{12/13}$ (Supplemental Figure 1).

$G\alpha_{12/13}$ proteins share a common downstream effector, the RGS domain-containing RhoGEF family of proteins (Fukuhara *et al.*, 2000; Booden *et al.*, 2002; Vogt *et al.*, 2003). There are three known mammalian RGS-containing RhoGEFs: PDZ-RhoGEF, found abundantly in brain (Swiercz *et al.*, 2002); p115-RhoGEF, which is highly expressed in hematopoietic cells (Whitehead *et al.*, 1996; Girkontaite *et al.*, 2001); and LARG, which seems to be ubiquitously expressed (Swiercz *et al.*, 2002). Interestingly, RNA-mediated knockdown of LARG robustly inhibited wounding-induced cell

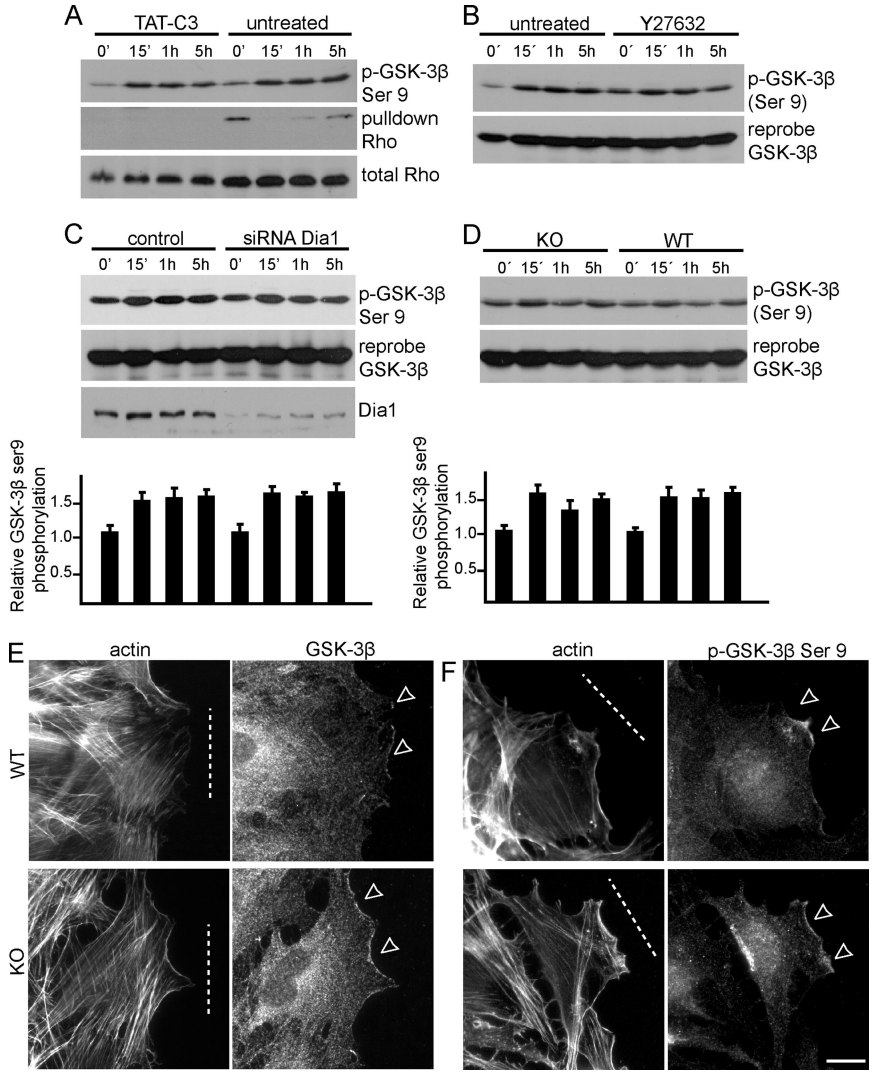

Figure 4. $G\alpha_{12/13}$ and RhoA-mDia1 are not involved in GSK-3β regulation. (A) WT MEFs were treated with TAT-C3, scratch-wounded for the times indicated, and subjected to Rho pull-down analysis. Cell extracts were immunoblotted to visualize RhoA or serine 9 phosphorylation of GSK-3β. (B) Immunoblot analysis of wound-induced GSK-3β serine 9 phosphorylation and reprobe for GSK-3β after treatment of WT cells with Y27632. (C) WT cells transfected with siRNA against mDia1 and immunoblotted for the indicated proteins. (D) Immunoblot analysis of GSK-3β or the serine 9 phosphorylated form in WT and KO cells from a scratch-induced time course experiment. (C and D) Densitometric quantifications of three independent experiments are shown together with representative Western blots; error bars represent SEM. (E) Representative images of actin and GSK-3β localization in wound-edge WT and KO cells (6 h after wounding). (F) Representative images of actin and GSK-3β serine 9-phosphorylated localization in wound-edge WT and KO cells (6 h after wounding). Dotted white lines represent the wound, and white arrows show areas of interest. Bar, 10 μm.

migration compared with control siRNA-transfected cells (Supplemental Movies 1 and 2 and Figure 2, A–C). This phenotype seemed to be comparable with the migration pattern and overall morphological appearance of $G\alpha_{12/13}$-deficient cells, albeit less severe. Next, we investigated whether LARG may also regulate cell polarity. We performed MTOC stainings in WT MEFs transfected with control (Figure 2E) or LARG-specific siRNA against the 3′ UTR of LARG (Figure 2F). Indeed, MTOC reorientation was severely affected in the LARG-knockdown cells compared with control siRNA-treated cells (Figure 2D). Similar data were obtained in NIH3T3 cells (Supplemental Figure 2). Reexpression of full-length LARG in cells treated with siRNA rescued MTOC polarity, confirming the role of LARG in the process (Figure 2, G and H).

The requirement of $G\alpha_{12/13}$ and LARG for MTOC polarization led us to investigate the functional role of RhoA in this process. Recently, Rho signaling through Diaphanous was shown to stabilize adherens junctions via catenin–cadherin complex formation (Sahai and Marshall, 2002). However, loss of cell-cell contacts was observed 4 h after wounding in $G\alpha_{12/13}$-deficient MEFs (Goulimari *et al*., 2005), coinciding with MTOC reorientation defects. We therefore compared β-catenin localization, and we found that cell-cell contacts were disorganized and less abundant in $G\alpha_{12/13}$-deficient cells (Figure 3, A and B). However, calcium depletion in WT cells resulted in relocalization of β-catenin to the cytoplasm (Figure 3C), but they did not have an effect on MTOC reorientation (Figure 3I).

To characterize the role of RhoA in cell polarity, we used the cell-permeable Rho inhibitory toxin TAT-C3 (Figure 3H) and siRNA against RhoA (Figure 3G). As shown in Figure 3I, MTOC polarization was inhibited by both TAT-C3 and siRNA against RhoA but not by 10 μM of the ROCK inhibitor Y27632 (Figure 3, D, F, and I). These results were confirmed in NIH3T3 fibroblasts (Supplemental Figure 2, A–J).

Recently, it was suggested that Cdc42 is not necessary during directed migration (Czuchra *et al*., 2005). However, in this study in vitro differentiated Cdc42-deficient fibroblasts were used that could have developed compensatory mechanisms. In fact, the specific requirement for Cdc42 in cell polarity was confirmed in MEFs derived from Cdc42$-/-$ embryos (Yang *et al*., 2006). We tested the involvement of Cdc42 in our cell system by using RNA interference. Of notice, siRNA against Cdc42 confirmed its requirement for MTOC reorientation (Figure 3, E and I) and directed migration (data not shown).

A well described signaling cascade in MTOC reorientation is Cdc42-dependent phosphorylation of GSK-3β at serine 9. This phosphorylation leads to GSK-3β inhibition and subse-

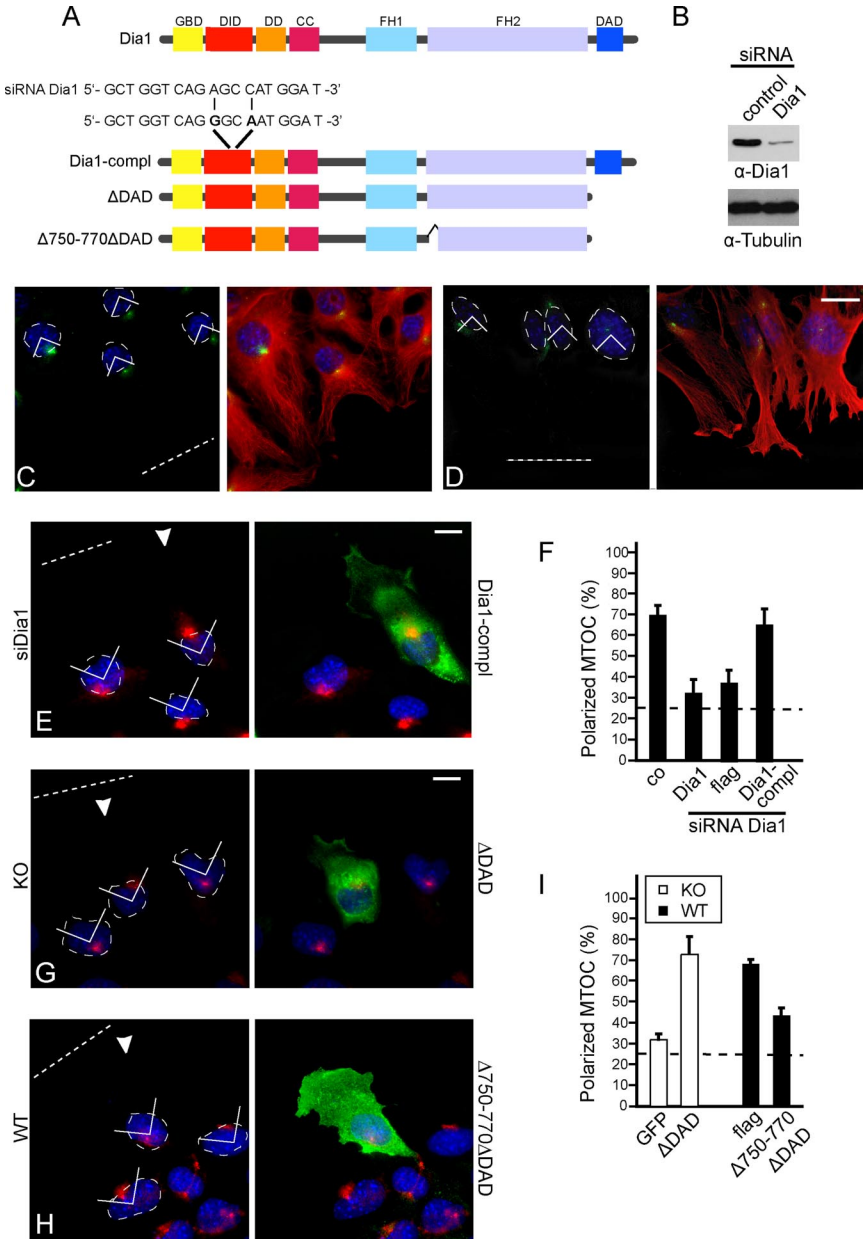

Figure 5. mDia1 regulates MTOC polarity. (A) Domain organization of mDia1 (GBD, GTPase-binding domain; DID, Dia inhibitory domain; DD, dimerization domain; CC, coiled coil; FH1, formin homology 1 domain). Dia1-compl contains the two point mutations A711G and C714A (positions 10 and 13 in the siRNA target sequence). (B) Cell lysates were immunoblotted for mDia1. Representative image of WT cells treated with control siRNA (C) and siRNA against mDia1 (D) stained for MTOC (green), DAPI (blue) and merged with α-tubulin (red). (E) Representative image of a WT cell treated with siRNA against mDia1 and microinjected with Dia1-compl (green, arrow). Image shows MTOC (red) and DAPI (blue). (F) Quantification of positive MTOCs after expression of the indicated constructs. Data represent means ± SEM of three independent experiments (total of 60 cells). (G) Representative image of a KO cell microinjected with ΔDAD (green, arrow) and stained for MTOC (red) and DAPI (blue). (H) Representative image of a WT cell microinjected with Δ750-770ΔDAD (green; arrow) and stained for MTOC (red) and DAPI (blue). (I) Quantification of polarized MTOCs after expression of the indicated constructs. Data represent means ± SEM of three independent experiments (total of 70–75 cells for each construct). Bar, 10 μm. The wound is indicated by a dotted line.

quent localization at the leading edge of migrating rat astrocytes, where it interacts with APC (Etienne-Manneville and Hall, 2003). Hence, we investigated GSK-3β phosphorylation during scratch-induced migration in WT and $G\alpha_{12/13}$-deficient MEFs. Overnight incubation with 0.2 μM TAT-C3 had no effect on serine 9 phosphorylation of GSK-3β in WT cells (Figure 4A), despite the ablation of RhoA activity (Figure 3H). Consistent with this, inhibition of ROCK or down-regulation of mDia1 also had no effect (Figure 4, B and C). Furthermore, we did not observe significant differences in the levels or localizations of GSK-3β or its phosphorylated form in wounded WT or $G\alpha_{12/13}$-deficient MEFs (Figure 4, D–F). These data implicate a role for $G\alpha_{12/13}$ and RhoA-mDia1 signaling in MTOC reorientation in addition to or in cooperation with Cdc42 and GSK-3β function.

To determine whether the RhoA effector mDia1 might be involved in MTOC polarity, we used siRNA against mDia1 (Figure 5B). Depletion of mDia1 by siRNA resulted in inhibition of MTOC reorientation (Figure 5, C–F) in line with previous observations (Yamana *et al.*, 2006). Furthermore, reintroduction of an mDia1 mutant (Dia1-compl) resistant to the siRNA used (Figure 5A) rescued MTOC reorientation in these cells (Figure 5, E and F). To better characterize the involvement of mDia1 in cell polarity we used mDia1 constructs lacking the Dia-autoinhibitory-domain (DAD) (Figure 5A) that is necessary to maintain the dormant protein conformation. Microinjection of ΔDAD in leading edge $G\alpha_{12/13}$-deficient cells promoted MTOC reorientation compared with control (Figure 5, G and I). To investigate whether mDia1-induced actin assembly was necessary, we expressed a mDia1 ΔDAD construct lacking amino acids 750–770 (Figure 5A), a region required for formin homology 2 (FH2) domain homodimerization and subsequent in vivo and in vitro actin polymerization (Copeland and Treisman, 2002; Copeland *et al.*, 2004). Interestingly, this construct inhibited MTOC reorientation in wild-type cells (Figure 5, H

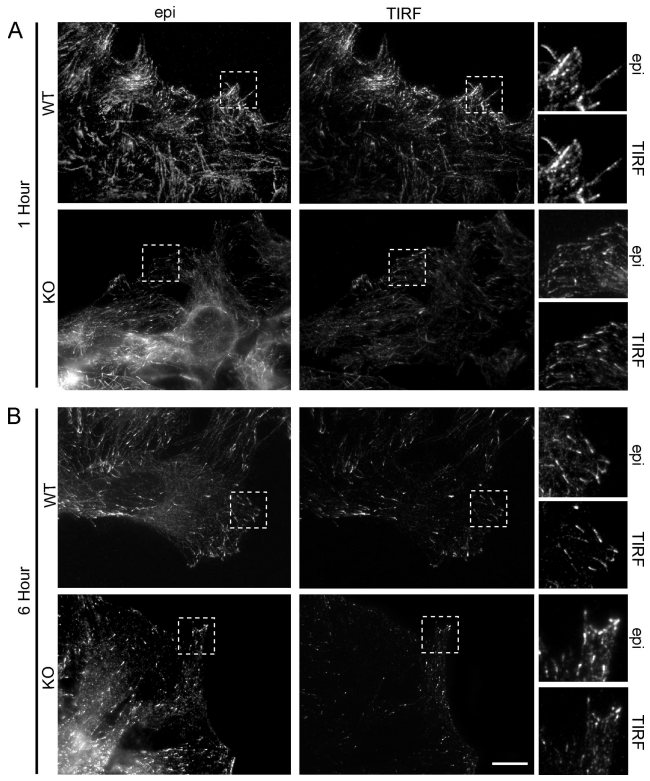

Figure 6. Comparative study of EB1 localization in WT and G$\alpha_{12/13}$-deficient MEFs using epifluorescence and TIRF microscopy. (A) Shown are representative epifluorescence and corresponding TIRF images of WT and KO leading edge cells, respectively, stained with α-EB1 to visualize the plus-end of microtubules at the cell membrane at 1 h after wounding. (B) Epifluorescence and TIRF images of WT and KO cells, respectively, 6 h after wounding. Areas marked within a dotted square are shown in magnification. Bar, 10 μm.

and I), and as may be expected inhibited cell migration (data not shown).

MTOC reorientation is affected in the G$\alpha_{12/13}$-deficient cells at 4 h after wounding. However, migrating MEFs must reorganize their microtubule cytoskeleton much earlier, because WT cells move immediately after wounding. To determine early changes in microtubules we studied microtubule dynamics in the G$\alpha_{12/13}$-deficient MEFs at 1 h after wounding. First, we analyzed the distribution of endogenous EB1. Both epifluorescence microscopy and TIRF microscopy revealed that there were fewer and less distinct EB1 positive dashes in the G$\alpha_{12/13}$-deficient cells compared with the WT cells, in particular, at 1 h after wounding (Figure 6). These data indicate that the microtubule cytoskeleton is deregulated in the G$\alpha_{12/13}$-deficient MEFs at time points where MTOC reorientation is not yet affected.

To directly characterize changes in microtubule dynamics, we monitored GFP-EB1 by TIRF microscopy after microinjection. TIRF microscopy shows enhanced sensitivity because it minimizes out-of focus signal from regions inside the cell. This allowed us to image low-expressing cells and to exclude possible microtubule stabilization effects due to overexpression of EB1. Live-cell imaging revealed GFP-EB1 as moving dashes that indicates microtubule-end growth (Supplemental Movies 3–6). Figure 7A shows the maximum projection (see *Materials and Methods*) of a time-lapse sequence of WT cells. The EB1-positive microtubule plus-ends move in a polarized manner in parallel tracks toward the leading edge (Figure 7A and Supplemental Movie 3). In G$\alpha_{12/13}$-deficient MEFs, EB1 dynamics were aberrant (Supplemental Movie 4). Although some EB1 dashes move toward the leading edge (Figure 7B), the majority of dashes move in an unpolarized manner. To look closer at the behavior of EB1-positive microtubules, we analyzed the movies frame by frame. Figure 7C shows that in WT cells, EB1 labeling is visible as distinct, fast-moving dashes, which persist for three to four frames. In comparison, EB1 dashes in G$\alpha_{12/13}$-deficient cells are less motile (Figure 7D). Kymographic analysis of the movies allowed for direct assessment of the EB1 tracks and velocity. Figures 7E and 8F show the representative areas, illustrated by the dotted rectangle, analyzed by a kymograph for WT and G$\alpha_{12/13}$-deficient cells, respectively. The angle of the EB1 traces in the kymograph is a direct measure for the microtubule advance rate. The resulting velocities show that microtubule plus-ends in G$\alpha_{12/13}$-deficient cells move significantly slower, with a mean velocity of 4.4 μm/min $\pm$ 0.5 compared with the WT cell velocity of 10.8 μm/min $\pm$ 0.8 (Figure 7G).

To study the role of mDia1 in microtubule dynamics, we looked at EB1 dynamics after treatment with siRNA against mDia1. Leading edge cells depleted of mDia1 were microinjected with GFP-EB1 and monitored with TIRF (Supplemental Movies 5 and 6), and representative kymographs show that microtubule advance was slower than in the control siRNA-treated cells (Figure 7, H–J). Together, these data indicate that G$\alpha_{12/13}$ proteins regulate microtubule dynamics during directed cell migration.

To confirm our findings, we followed GFP-EB1 dynamics in live WT (Figure 8A) and KO cells (Figure 8B) with epifluorescence microscopy. Dynamic imaging revealed GFP-EB1 moving dashes indicative of microtubule-end growth (Supplemental Movies 7 and 8). To calculate the velocity of the migrating EB1 comets, we used manual tracking, which confirmed that EB1 comets migrate slower in the G$\alpha_{12/13}$-deficient cells (5.8 μm/min), compared with the WT cells (11.2 μm/min) (Figure 8C).

To verify the differences observed in microtubule dynamics, we analyzed another microtubule tip-binding protein, EB3-GFP, that was previously used to visualize microtubule growth (Stepanova *et al*., 2003). Time-lapse imaging of EB3-GFP in WT (Figure 6D and Supplemental Movie 9) and KO cells (Figure 8E and Supplemental Movie 10) showed that EB3 comets migrate slower in the G$\alpha_{12/13}$-deficient cells (6.2 μm/min) than in the WT cells (11.8 μm/min) (Figure 8F).

A recent study in *Drosophila* S2 cells reported that DRhoGEF2 is localized at the centrosome and that it is transported to the cell cortex along microtubules in an EB1-dependent manner. We hypothesized that the mammalian homologue LARG may be regulated in a similar manner. To test this, we performed immunoprecipitation studies and found that LARG efficiently coimmunoprecipitated with pericentrin (Figure 9A) but not with EB1 (data not shown), suggesting that LARG regulates MTOC polarity by interactions with pericentrin. Immunoprecipitations with either the N terminus of LARG containing the first 820 amino acids (LARG-NT) or the C terminus of LARG containing amino acids 1131–1544 (LARG-CT) revealed that the interaction occurs within the N-terminal half of LARG (Figure 9, A and B). Interestingly, using spinning disk confocal microscopy we observed LARG colocalization with pericentrin in wounded, polarized fibroblasts (Figure 9C).

Next, we microinjected leading edge WT and G$\alpha_{12/13}$-deficient MEFs with GFP or GFP-LARG, stained for α-tubulin, and then analyzed the cells by TIRF microscopy, which

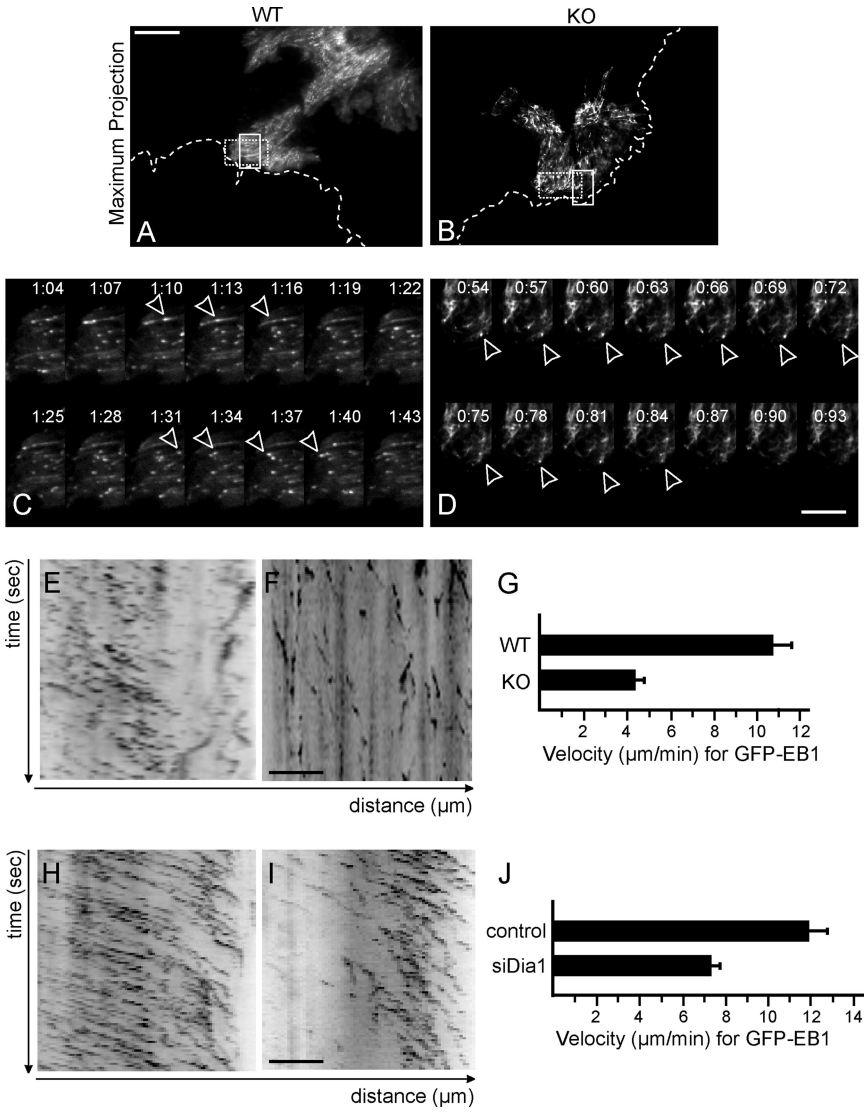

Figure 7. EB1 dynamics are disturbed in the $G\alpha_{12/13}$-deficient fibroblasts. (A) Maximum intensity projection image of GFP-EB1 in a WT leading edge cell (Supplemental Movie 3). (B) Maximum projection image of GFP-EB1 in a KO cell (Supplemental Movie 4). White dotted line represents the wound. Bar, 10 μm. (C) The sequence of images shows EB1 behavior in a WT cell at a 3-s interval and represents the area within the white rectangle in A. (D) Sequence showing EB1 in a KO cell from the area within the white rectangle in B. Bar, 5 μm. (E) Kymographic analysis of GFP-EB1 in a WT cell showing time (seconds) on the *y*-axis and distance (micrometers) traveled on the *x*-axis, representing the area within the dotted rectangle in A. (F) Kymographic analysis of GFP-EB1 in a KO cell from the area within the dotted rectangle in B. Bar, 5 μm. (I) Graph showing the velocity in μm/min of GFP-EB1 in WT and KO cells. Error bars represent SEM (6 cells analyzed in each example). (H) Kymographic analysis of GFP-EB1 in WT cells treated with control siRNA (Supplemental Movie 5). (I) Kymograph of GFP-EB1 in WT cells treated with siRNA against mDia1 (Supplemental Movie 6). (J) Graph showing the velocity of migrating EB1 dashes in WT cells treated with siRNA against the indicated proteins. Error bars show SEM (6 cells analyzed in each example).

allows for analysis close to the cell cortex. This revealed that GFP-LARG showed a pattern reminiscent of microtubule tracks extending toward the cell front in WT cells (Figure 9D). However, this was not observed when GFP-tagged constructs containing either the PDZ-RGS or the RGS domain alone were used (Supplemental Figure 3). When we

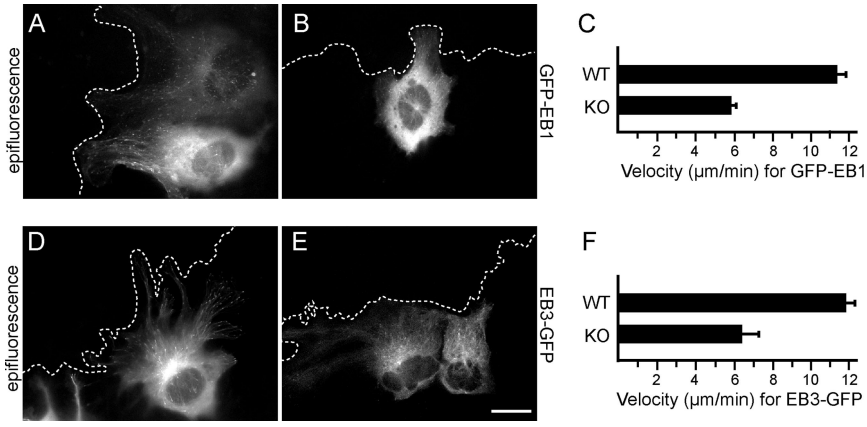

Figure 8. Comparative study of EB1 and EB3 dynamics with epifluorescence time-lapse imaging. (A) Epifluorescence image of a WT cell expressing GFP-EB1 after microinjection. The image corresponds to Supplemental Movie 7. (B) Epifluorescence image of a KO cell expressing GFP-EB1 after microinjection corresponding to Supplemental Movie 8. (C) Graph shows the mean velocity of GFP-EB1 comets as measured with manual tracking (see *Materials and Methods*) in micrometers per minute. (D) Epifluorescence image of a WT cell microinjected with EB3-GFP. The image corresponds to Supplemental Movie 9. (E) Epifluorescence image of a KO cell expressing EB3-GFP after microinjection corresponding to Supplemental Movie 10. (F) Graph shows the mean velocity of EB3-GFP comets in micrometers per minute. Five cells were analyzed for each experiment. Bar, 3 μm.

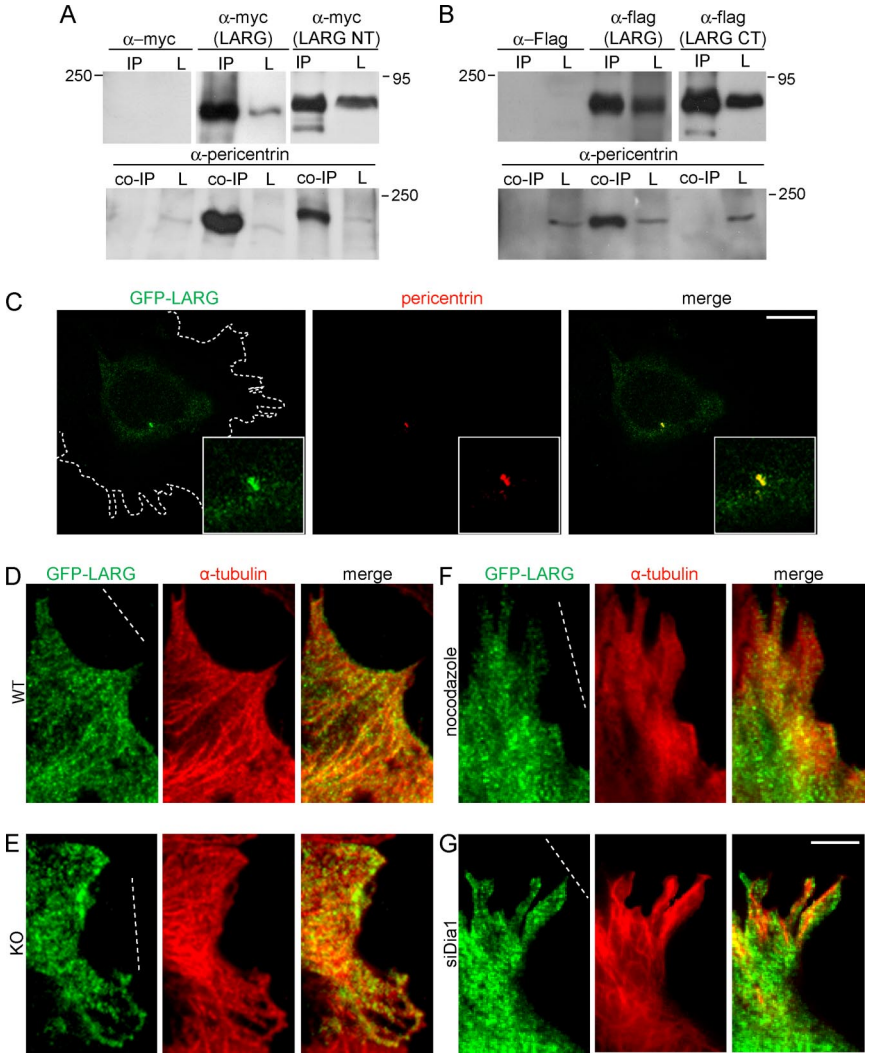

Figure 9. LARG associates with pericentrin, and it is localized along microtubule tracks. (A) HEK cells were transfected with myc, myc-LARG, or myc-LARG NT, and they were subjected to immunoprecipitation (IP). Input is shown to the right (L, lysate) and represents 10% of total cell lysate (top lane). Coimmunoprecipitation with endogenous pericentrin (coIP) is shown in the bottom lane. Fifty percent of total IP was loaded on gel for each example shown. (B) HEK cells were transfected with flag, flag-LARG, or flag-LARG CT, and they were subjected to IP. Input is shown to the right (L) and represents 10% of total cell lysate (top lane). CoIP endogenous pericentrin is shown in the bottom lane. Fifty percent of total IP was loaded on gel for each example shown. Molecular weight marker (kilodaltons) is shown to the left or right of each panel. (C) WT MEFs were microinjected with GFP-LARG. Representative image of a 0.3-μm Z section from a spinning disk confocal sequence showing GFP-LARG, pericentrin (red) staining, and merged is shown. The outline of the cell is shown in a dotted line. Insets show the area of colocalization in a higher magnification. Bar, 1 μm. Leading edge WT (D) and KO (E) were microinjected with GFP-LARG. Shown are representative TIRF images of GFP-LARG, α-tubulin (red), and merged images. (F) Leading WT MEFs were microinjected with GFP-LARG and immediately treated with 2 μM nocodazole for 1.5 h. Shown are representative TIRF images of GFP-LARG, α-tubulin staining (red), and merged. (G) WT MEFs were treated with siRNA against mDia1. Leading edge cells were microinjected with GFP-LARG and representative images as shown with α-tubulin (red) and merged. Bar, 3 μm. The wound is indicated by a dotted line. In total, seven cells were analyzed in each example.

looked at GFP-LARG localization in G$\alpha_{12/13}$-deficient MEFs, some tracks were still visible, albeit less distinct, and not generally toward the front of the cell (Figure 9E). LARG localization along microtubule tracks was also sensitive to nocodazole treatment or RNA interference against mDia1 (Figure 9, F and G).

DISCUSSION

In this study, we identified a G$\alpha_{12/13}$ signal transduction pathway involving LARG and mDia1 that regulates microtubule-based cell polarity in mammalian cells. The presence of serum components activating G$\alpha_{12/13}$-coupled receptors such as LPA may, therefore, be important in regulating microtubule dynamics in directional cell movement.

How could G$\alpha_{12/13}$ activation control microtubules? Our data suggest a model where the G$\alpha_{12/13}$-regulated RhoGEF LARG is associated with the microtubule cytoskeleton, which may localize the RhoGEF for activation at the cell cortex. Interestingly, LARG has recently been shown to associate with mDia1 in a feedback module, suggesting a tight mechanistic control of both proteins for cell morphological events (Kitzing *et al.*, 2007). Our data suggest that mDia1 may influence microtubule behavior by locally controlled actin assembly. This is supported by the fact that a ΔDAD-mDia1 mutant deficient in actin polymerization inhibits MTOC orientation in wild-type cells, whereas the active variant ΔDAD promotes polarity in G$\alpha_{12/13}$-deficient cells. The role of mDia1 in cell polarity is further emphasized by the fact that it directly associates with the microtubule-regulating and MTOC polarizing protein IQGAP1 (Fukata *et al.*, 2002; Watanabe *et al.*, 2004), which also recruits active mDia1 to the front of migrating cells for localized actin polymerization (Brandt and Grosse, 2007; Brandt *et al.*, 2007). However, the involvement of mDia1-mediated actin rearrangement could also be due to its requirement for the production of extensions needed for orientation toward the wound and subsequent microtubule rearrangement.

A study by Eng *et al.* (2006) showed that mDia1 can regulate the Par6-aPKC target GSK-3β. We studied GSK-3β regulation in WT, G$\alpha_{12/13}$-deficient, and RhoA- and mDia1-depleted MEFs to determine whether there is cross talk between the GSK-3β pathway and G$\alpha_{12/13}$ signaling in our cell system, but we found no significant differences. This independence of RhoA signaling is in line with previous studies in astrocytes (Etienne-Manneville and Hall, 2003). However, we cannot exclude the possibility that G$\alpha_{12/13}$-Rho-mDia1 signaling is influenced by GSK-3β.

When we assessed the influence of G$\alpha_{12/13}$ on the dynamics of EB1 in G$\alpha_{12/13}$-deficient MEFs, we observed that EB1

localization at the plus-ends of growing microtubules was sparse during cell migration. Dynamic imaging of GFP-EB1 positive microtubules revealed that the advancement rate was slower and less directed toward the wound edge in $G\alpha_{12/13}$-deficient cells as early as 90 min after wounding. We speculate that these altered microtubule dynamics could account for the failure to reorient the MTOC in the $G\alpha_{12/13}$-deficient cells, which becomes evident at later time points. A recent study in *Caenorhabditis elegans* supports this scenario, demonstrating how growing microtubules come into direct contact with specific sites at the cortex before depolymerizing, and computational analysis showed that the generated forces are able to pull the mitotic spindle into the right position (Kozlowski *et al*., 2007). The altered microtubule advancement rates in $G\alpha_{12/13}$-deficient or mDia1-depleted cells point to a role of EB1 beyond its role in APC-mediated microtubule stabilization. This is also suggested by a recent study showing that EB1 colocalizes only partially and to a very small extend to APC at the tip of microtubules and that this interaction occurs only transiently (Kita *et al*., 2006). In addition, EB1 depletion studies in both mouse fibroblasts and *Drosophila* S2 cells suggest that EB1 promotes microtubule dynamics independent of APC (Rogers *et al*., 2002; Kita *et al*., 2006). We see that EB1 localization and dynamics are regulated by $G\alpha_{12/13}$ signaling.

The RGS domain-containing protein LARG has been implicated in mediating RhoA activation downstream of GPCRs and $G\alpha_{12/13}$ through its ability to directly interact with $G\alpha$ subunits (Reuther *et al*., 2001; Booden *et al*., 2002). Nevertheless, its biological importance has remained poorly understood. We used RNA interference against LARG and revealed its involvement in cell polarity. Initial evidence for the involvement of RGS-domain containing RhoGEFs in cell polarity came from studies in *Drosophila* S2 cells where the LARG homologue DRhoGEF2 was shown to act downstream of the trimeric G protein Concertina to induce shape change during gastrulation and morphogenesis (Parks and Wieschaus, 1991; Barrett *et al*., 1997; Halsell *et al*., 2000). In the present study, we show that in mammalian cells LARG interacts and colocalizes with pericentrin and may be dynamically regulated to the cell cortex via microtubules, suggesting a comparable scenario like in *Drosophila* cells, where DRhoGEF2 is transported to the cell cortex in an EB1-dependent manner (Rogers *et al*., 2004). However, different mechanisms must be at work in mammalian cells because we did not observe interaction of LARG with EB1. Interestingly, we found that mDia1 is required for the localization of LARG along microtubules. Hence, the function of mDia1 in microtubule dynamics may feed back into the efficient localized distribution of LARG during directional cell movement. Clearly, further studies are necessary to reveal the precise nature of the interaction between LARG and the microtubule cytoskeleton and to identify the proteins that might be involved in its transport to the cortex.

Cell polarity during migration is a very dynamic event involving a range of proteins and mechanisms. Our data implicate that $G\alpha_{12/13}$ regulate microtubule dynamics and cell polarity during migration in mammalian cells in a RhoGEF and formin-dependent manner.

ACKNOWLEDGMENTS

We thank B. Di Ventura and E. T. Bodor for critical reading of the manuscript. We are grateful to S. Gutkind (NIH, Bethesda, MD) for providing GFP-LARG and N. Galjart (Erasmus Medical Centre, Rotterdam, The Netherlands) for EB3-GFP. We thank A. Rippberger for technical assistance and the Nikon Imaging Center at the University of Heidelberg for providing microscope equipment. This work was supported by the Emmy Noether Program of the Deutsche Forschungsgemeinschaft GR 2111/1-2 (to R.G.).

REFERENCES

Akhmanova, A., and Hoogenraad, C. C. (2005). Microtubule plus-end-tracking proteins: mechanisms and functions. Curr. Opin. Cell Biol. *17*, 47–54.

Arakawa, Y., Bito, H., Furuyashiki, T., Tsuji, T., Takemoto-Kimura, S., Kimura, K., Nozaki, K., Hashimoto, N., and Narumiya, S. (2003). Control of axon elongation via an SDF-1alpha/Rho/mDia pathway in cultured cerebellar granule neurons. J. Cell Biol. *161*, 381–391.

Barrett, K., Leptin, M., and Settleman, J. (1997). The Rho GTPase and a putative RhoGEF mediate a signaling pathway for the cell shape changes in *Drosophila* gastrulation. Cell *91*, 905–915.

Birkenfeld, J., Nalbant, P., Bohl, B. P., Pertz, O., Hahn, K. M., and Bokoch, G. M. (2007). GEF-H1 modulates localized RhoA activation during cytokinesis under the control of mitotic kinases. Dev. Cell *12*, 699–712.

Booden, M. A., Siderovski, D. P., and Der, C. J. (2002). Leukemia-associated Rho guanine nucleotide exchange factor promotes G alpha q-coupled activation of RhoA. Mol. Cell Biol. *22*, 4053–4061.

Brandt, D. T., and Grosse, R. (2007). Get to grips: steering local actin dynamics with IQGAPs. EMBO Rep. *8*, 1019–1023.

Brandt, D. T., Marion, S., Griffiths, G., Watanabe, T., Kaibuchi, K., and Grosse, R. (2007). Dia1 and IQGAP1 interact in cell migration and phagocytic cup formation. J. Cell Biol. *178*, 193–200.

Copeland, J. W., Copeland, S. J., and Treisman, R. (2004). Homo-oligomerization is essential for F-actin assembly by the formin family FH2 domain. J. Biol. Chem. *279*, 50250–50256.

Copeland, J. W., and Treisman, R. (2002). The diaphanous-related formin mDia1 controls serum response factor activity through its effects on actin polymerization. Mol. Biol. Cell *13*, 4088–4099.

Czuchra, A., Wu, X., Meyer, H., van Hengel, J., Schroeder, T., Geffers, R., Rottner, K., and Brakebusch, C. (2005). Cdc42 is not essential for filopodium formation, directed migration, cell polarization, and mitosis in fibroblastoid cells. Mol. Biol. Cell *16*, 4473–4484.

Dictenberg, J. B., Zimmerman, W., Sparks, C. A., Young, A., Vidair, C., Zheng, Y., Carrington, W., Fay, F. S., and Doxsey, S. J. (1998). Pericentrin and gamma-tubulin form a protein complex and are organized into a novel lattice at the centrosome. J. Cell Biol. *141*, 163–174.

Doxsey, S. J., Stein, P., Evans, L., Calarco, P. D., and Kirschner, M. (1994). Pericentrin, a highly conserved centrosome protein involved in microtubule organization. Cell *76*, 639–650.

Eng, C. H., Huckaba, T. M., and Gundersen, G. G. (2006). The Formin mDia regulates GSK3{beta} through novel PKCs to promote microtubule stabilization but not MTOC reorientation in migrating fibroblasts. Mol. Biol. Cell *17*, 5004–5016.

Etienne-Manneville, S., and Hall, A. (2003). Cdc42 regulates GSK-3beta and adenomatous polyposis coli to control cell polarity. Nature *421*, 753–756.

Faix, J., and Grosse, R. (2006). Staying in shape with formins. Dev. Cell *10*, 693–706.

Fukata, M., Nakagawa, M., and Kaibuchi, K. (2003). Roles of Rho-family GTPases in cell polarisation and directional migration. Curr. Opin. Cell Biol. *15*, 590–597.

Fukata, M., Watanabe, T., Noritake, J., Nakagawa, M., Yamaga, M., Kuroda, S., Matsuura, Y., Iwamatsu, A., Perez, F., and Kaibuchi, K. (2002). Rac1 and Cdc42 capture microtubules through IQGAP1 and CLIP-170. Cell *109*, 873–885.

Fukuhara, S., Chikumi, H., and Gutkind, J. S. (2000). Leukemia-associated Rho guanine nucleotide exchange factor (LARG) links heterotrimeric G proteins of the G(12) family to Rho. FEBS Lett. *485*, 183–188.

Galjart, N., and Perez, F. (2003). A plus-end raft to control microtubule dynamics and function. Curr. Opin. Cell Biol. *15*, 48–53.

Girkontaite, I., Missy, K., Sakk, V., Harenberg, A., Tedford, K., Potzel, T., Pfeffer, K., and Fischer, K. D. (2001). Lsc is required for marginal zone B cells, regulation of lymphocyte motility and immune responses. Nat. Immunol. *2*, 855–862.

Goulimari, P., Kitzing, T. M., Knieling, H., Brandt, D. T., Offermanns, S., and Grosse, R. (2005). Galpha12/13 is essential for directed cell migration and localized Rho-Dia1 function. J. Biol. Chem. *280*, 42242–42251.

Grosse, R., Copeland, J. W., Newsome, T. P., Way, M., and Treisman, R. (2003). A role for VASP in RhoA-Diaphanous signalling to actin dynamics and SRF activity. EMBO J. *22*, 3050–3061.

Grosse, R., Roelle, S., Herrlich, A., Hohn, J., and Gudermann, T. (2000). Epidermal growth factor receptor tyrosine kinase mediates Ras activation by gonadotropin-releasing hormone. J. Biol. Chem. *275*, 12251–12260.

Gudermann, T., Grosse, R., and Schultz, G. (2000). Contribution of receptor/G protein signaling to cell growth and transformation. Naunyn Schmiedebergs Arch. Pharmacol. *361*, 345–362.

Habas, R., Kato, Y., and He, X. (2001). Wnt/Frizzled activation of Rho regulates vertebrate gastrulation and requires a novel Formin homology protein Daam1. Cell *107*, 843–854.

Halsell, S. R., Chu, B. I., and Kiehart, D. P. (2000). Genetic analysis demonstrates a direct link between rho signaling and nonmuscle myosin function during *Drosophila* morphogenesis. Genetics *155*, 1253–1265.

Kelly, P., Moeller, B. J., Juneja, J., Booden, M. A., Der, C. J., Daaka, Y., Dewhirst, M. W., Fields, T. A., and Casey, P. J. (2006a). The G12 family of heterotrimeric G proteins promotes breast cancer invasion and metastasis. Proc. Natl. Acad. Sci. USA *103*, 8173–8178.

Kelly, P., Stemmle, L. N., Madden, J. F., Fields, T. A., Daaka, Y., and Casey, P. J. (2006b). A role for the G12 family of heterotrimeric G proteins in prostate cancer invasion. J. Biol. Chem. *281*, 26483–26490.

Kiosses, W. B., McKee, N. H., and Kalnins, V. I. (1997). Relationship between the distribution of stress fibers and centrosomes in endothelial cells of the rat aorta. Cell Motil. Cytoskeleton *36*, 228–235.

Kita, K., Wittmann, T., Nathke, I. S., and Waterman-Storer, C. M. (2006). Adenomatous polyposis coli on microtubule plus ends in cell extensions can promote microtubule net growth with or without EB1. Mol. Biol. Cell *17*, 2331–2345.

Kitzing, T. M., Sahadevan, A. S., Brandt, D. T., Knieling, H., Hannemann, S., Fackler, O. T., Grosshans, J., and Grosse, R. (2007). Positive feedback between Dia1, LARG, and RhoA regulates cell morphology and invasion. Genes Dev. *21*, 1478–1483.

Kozlowski, C., Srayko, M., and Nedelec, F. (2007). Cortical microtubule contacts position the spindle in *C. elegans* embryos. Cell *129*, 499–510.

Kreutz, B., Hajicek, N., Yau, D. M., Nakamura, S., and Kozasa, T. (2007). Distinct regions of Galpha13 participate in its regulatory interactions with RGS homology domain-containing RhoGEFs. Cell Signal. *19*, 1681–1689.

Ligon, L. A., Shelly, S. S., Tokito, M., and Holzbaur, E. L. (2003). The microtubule plus-end proteins EB1 and dynactin have differential effects on microtubule polymerization. Mol. Biol. Cell *14*, 1405–1417.

Lin, F., Sepich, D. S., Chen, S., Topczewski, J., Yin, C., Solnica-Krezel, L., and Hamm, H. (2005). Essential roles of G{alpha}12/13 signaling in distinct cell behaviors driving zebrafish convergence and extension gastrulation movements. J. Cell Biol. *169*, 777–787.

Luders, J., and Stearns, T. (2007). Microtubule-organizing centres: a re-evaluation. Nat. Rev. Mol. Cell Biol. *8*, 161–167.

Mimori-Kiyosue, Y., and Tsukita, S. (2003). "Search-and-capture" of microtubules through plus-end-binding proteins (+TIPs). J. Biochem. *134*, 321–326.

Moissoglu, K., and Schwartz, M. A. (2006). Integrin signalling in directed cell migration. Biol. Cell *98*, 547–555.

Offermanns, S. (2003). G-proteins as transducers in transmembrane signalling. Prog. Biophys. Mol. Biol. *83*, 101–130.

Palazzo, A. F., Joseph, H. L., Chen, Y. J., Dujardin, D. L., Alberts, A. S., Pfister, K. K., Vallee, R. B., and Gundersen, G. G. (2001). Cdc42, dynein, and dynactin regulate MTOC reorientation independent of Rho-regulated microtubule stabilization. Curr. Biol. *11*, 1536–1541.

Parks, S., and Wieschaus, E. (1991). The Drosophila gastrulation gene concertina encodes a G alpha-like protein. Cell *64*, 447–458.

Price, L. S., Langeslag, M., ten Klooster, J. P., Hordijk, P. L., Jalink, K., and Collard, J. G. (2003). Calcium signaling regulates translocation and activation of Rac. J. Biol. Chem. *278*, 39413–39421.

Reuther, G. W., Lambert, Q. T., Booden, M. A., Wennerberg, K., Becknell, B., Marcucci, G., Sondek, J., Caligiuri, M. A., and Der, C. J. (2001). Leukemia-associated Rho guanine nucleotide exchange factor, a Dbl family protein found mutated in leukemia, causes transformation by activation of RhoA. J. Biol. Chem. *276*, 27145–27151.

Rogers, S. L., Rogers, G. C., Sharp, D. J., and Vale, R. D. (2002). *Drosophila* EB1 is important for proper assembly, dynamics, and positioning of the mitotic spindle. J. Cell Biol. *158*, 873–884.

Rogers, S. L., Wiedemann, U., Hacker, U., Turck, C., and Vale, R. D. (2004). *Drosophila* RhoGEF2 associates with microtubule plus ends in an EB1-dependent manner. Curr. Biol. *14*, 1827–1833.

Rosenfeldt, H., Castellone, M. D., Randazzo, P. A., and Gutkind, J. S. (2006). Rac inhibits thrombin-induced Rho activation: evidence of a Pak-dependent GTPase crosstalk. J. Mol. Signal. *1*, 8.

Sahai, E., and Marshall, C. J. (2002). ROCK and Dia have opposing effects on adherens junctions downstream of Rho. Nat. Cell Biol. *4*, 408–415.

Sandblad, L., Busch, K. E., Tittmann, P., Gross, H., Brunner, D., and Hoenger, A. (2006). The *Schizosaccharomyces pombe* EB1 homolog Mal3p binds and stabilizes the microtubule lattice seam. Cell *127*, 1415–1424.

Stepanova, T., Slemmer, J., Hoogenraad, C. C., Lansbergen, G., Dortland, B., De Zeeuw, C. I., Grosveld, F., van Cappellen, G., Akhmanova, A., and Galjart, N. (2003). Visualization of microtubule growth in cultured neurons via the use of EB3-GFP (end-binding protein 3-green fluorescent protein). J. Neurosci. *23*, 2655–2664.

Strutt, D. I., Weber, U., and Mlodzik, M. (1997). The role of RhoA in tissue polarity and Frizzled signalling. Nature *387*, 292–295.

Su, L. K., Burrell, M., Hill, D. E., Gyuris, J., Brent, R., Wiltshire, R., Trent, J., Vogelstein, B., and Kinzler, K. W. (1995). APC binds to the novel protein EB1. Cancer Res. *55*, 2972–2977.

Swiercz, J. M., Kuner, R., Behrens, J., and Offermanns, S. (2002). Plexin-B1 directly interacts with PDZ-RhoGEF/LARG to regulate RhoA and growth cone morphology. Neuron *35*, 51–63.

Tanabe, S., Kreutz, B., Suzuki, N., and Kozasa, T. (2004). Regulation of RGS-RhoGEFs by Galpha12 and Galpha13 proteins. Methods Enzymol. *390*, 285–294.

Vogt, S., Grosse, R., Schultz, G., and Offermanns, S. (2003). Receptor-dependent RhoA activation in G12/G13-deficient cells: genetic evidence for an involvement of Gq/G11. J. Biol. Chem. *278*, 28743–28749.

Wang, H. R., Zhang, Y., Ozdamar, B., Ogunjimi, A. A., Alexandrova, E., Thomsen, G. H., and Wrana, J. L. (2003). Regulation of cell polarity and protrusion formation by targeting RhoA for degradation. Science *302*, 1775–1779.

Watanabe, N., Madaule, P., Reid, T., Ishizaki, T., Watanabe, G., Kakizuka, A., Saito, Y., Nakao, K., Jockusch, B. M., and Narumiya, S. (1997). p140mDia, a mammalian homolog of Drosophila diaphanous, is a target protein for Rho small GTPase and is a ligand for profilin. EMBO J. *16*, 3044–3056.

Watanabe, T., Wang, S., Noritake, J., Sato, K., Fukata, M., Takefuji, M., Nakagawa, M., Izumi, N., Akiyama, T., and Kaibuchi, K. (2004). Interaction with IQGAP1 links APC to Rac1, Cdc42, and actin filaments during cell polarization and migration. Dev. Cell *7*, 871–883.

Whitehead, I. P., Khosravi-Far, R., Kirk, H., Trigo-Gonzalez, G., Der, C. J., and Kay, R. (1996). Expression cloning of lsc, a novel oncogene with structural similarities to the Dbl family of guanine nucleotide exchange factors. J. Biol. Chem. *271*, 18643–18650.

Wittmann, T., and Waterman-Storer, C. M. (2001). Cell motility: can Rho GTPases and microtubules point the way? J. Cell Sci. *114*, 3795–3803.

Yamana, N. *et al*. (2006). The Rho-mDia1 pathway regulates cell polarity and focal adhesion turnover in migrating cells through mobilizing Apc and c-Src. Mol. Cell Biol. *26*, 6844–6858.

Yang, L., Wang, L., and Zheng, Y. (2006). Gene targeting of Cdc42 and Cdc42GAP affirms the critical involvement of Cdc42 in filopodia induction, directed migration, and proliferation in primary mouse embryonic fibroblasts. Mol. Biol. Cell *17*, 4675–4685.

Zimmerman, W., Sparks, C. A., and Doxsey, S. J. (1999). Amorphous no longer: the centrosome comes into focus. Curr. Opin. Cell Biol. *11*, 122–128.